Eur. J. Mineral.
2013, **25**, 61–70
Published online November 2012

Yukonite-like alteration products (Ca–Fe arsenate and As-rich Fe-oxyhydroxide) formed by *in situ* weathering in granodiorite, Bi'r Tawilah gold prospect, Saudi Arabia

ADEL A. SUROUR[1,2,*], AHMED H. AHMED[1,3] and HESHAM M. HARBI[1]

[1] Department of Mineral Resources and Rocks, Faculty of Earth Sciences, King Abdulaziz University, B.O. Box 80206, 21589 Jeddah, Saudi Arabia
[2] Department of Geology, Faculty of Science, Cairo University, Giza, Egypt
*Corresponding author, e-mail: aasurour63@hotmail.com
[3] Department of Geology, Faculty of Science, Helwan University, Ain Helwan, Egypt

Abstract: Samples from drilling of the Bi'r Tawilah gold prospect in Saudi Arabia reveal the occurrence of a Ca–Fe arsenate phase, which is similar in appearance and chemistry to yukonite. Upon weathering of a granodiorite host, oxidation of arsenopyrite (0–25 m deep) leads to the formation of a very peculiar brown, amorphous to very poorly crystalline aggregate with cellular-like texture. This mixture consists of Ca–Fe arsenate and arsenic-rich ferric oxyhydroxide resulting from the oxidation of arsenopyrite. It is intergrown with colloform ferric oxyhydroxide, the latter resulting from the oxidation of pre-existing pyrite. The EMPA analyses indicate that the Ca-rich domain contains the maximum As_2O_5 content (up to 22.3 wt%) whereas the colloform ferric oxyhydroxide contains the highest amount of Fe_2O_3 among the sample studied (60.8–63.1 wt%) associated to higher H_2O content (31.4–33.2 wt%) than in the case of common goethite and lepidocrocite. As far as typical yukonite, scorodite or arsenosiderite are absent in the studied weathered granodiorite, it is believed that oxidation took place at elevated pH (>7) and temperature up to ~75 °C. The source of Ca^{2+} can be derived from alteration of plagioclase in the granodiorite but its possible derivation from strongly corroded marble bands cannot be discarded. It is evident that availability of Ca^{2+} and high pH buffered by the dissolution of calcite in the marble, in addition to the prevailing temperature upon weathering, played important roles in the formation of these pseudomorphs at Bi'r Tawilah.

Key-words: amorphous, Ca–Fe arsenate, pseudomorph, *in situ* weathering, Bi'r Tawilah, Saudi Arabia.

1. Introduction

The most common primary arsenic minerals in nature are arsenic sulphides (arsenopyrite, arsenic-bearing pyrite, orpiment and realgar) whereas about 300–350 secondary arsenic minerals can be grouped into arsenic sulphides, arsenic (III) oxides (arsenites) and arsenic (V) oxides (arsenates) as shown by Drahota & Filippi (2009). The mobility of As^{3+} and As^{5+} in gold mine tailings and ground waters was the concern of several workers, *e.g.* Juillot *et al.* (1999), Saxena *et al.* (2004), Sigel *et al.* (2005) and Sigafusson *et al.* (2008). A recent detailed study by Walker *et al.* (2009a) on arsenic mobility and mineralogy in tailings and soils summarized that secondary mineral assemblages are rich in amorphous hydrous ferric arsenates (HFA), hydrous ferric oxyhydroxide (HFO) and Ca–Fe arsenates. The latter comprise crystalline yukonite [$Ca_7Fe_{12}(AsO_4)_{10}(OH)_{20}\cdot 15H_2O$] (Jambor, 1966) that can be formulated also as [$Ca_6Fe^{3+}_{16}(AsO_4)_{10}(OH)_{30}\cdot 23H_2O$] (Garavelli *et al.*, 2009) and arsenosiderite [$Ca_2Fe^{3+}_3(AsO_4)_3O_2\cdot 3H_2O$] (Dunn, 1979), in addition to Fe arsenates such as crystalline scorodite, kaňkite ($FeAsO_4\cdot 3.5H_2O$) and pharmacosiderite [$KFe_4(AsO_4)_3(OH)_{4.6-7}H_2O$], As-bearing ferric oxyhydroxides (mainly goethite, lepidocrocite and akaganeite) and finally As-bearing sulphates such as jarosite [$(K,Na,H_3O)Fe_3(SO_4)_2(OH)_6$] and tooeleite [$Fe_6(AsO_3)_4(SO)_4\cdot 4H_2O$] where the latter is an arsenite-sulphate phase.There are also rare Ca–Fe arsenates such as sewardite [$CaFe^{3+}{}_2(AsO_4)_2(OH)_2$] and kolfanite [$Ca_2Fe^{3+}_3O_2(AsO_4)_3\cdot 2H_2O$] in addition to some unnamed arseniosiderite-related phases (Walenta, 1998; Roberts *et al.*, 2002). The mineralogy of HFA, HFO and As-bearing sulphates depends on rate of oxidation during weathering, redox conditions and availability of elements such as Ca, Fe, K and Na. Gomez *et al.* (2009, 2010) succeeded for the first time in producing synthetic yukonite, which they compared to both natural yukonite and arsenosiderite.

The first report of yukonite as a new mineral species, from the Yukon Territory in Canada, was published by Tyrrell & Graham (1913). The mineral was later re-examined by Jambor (1966) who distinguished yukonite from

DOI: 10.1127/0935-1221/2013/0025-2246
0935-1221/13/0025-2246 $ 4.50

arseniosiderite. Generally, yukonite and similar minerals are rare and they can be detected in trace amounts in a number of occurrences in the world, especially gold mine wastes (*e.g*., Salzsauler *et al*., 2005; Filippi *et al*., 2007; Shuvaeva *et al*., 2007; Cano-Aguilera *et al*., 2008; de Andrade *et al*., 2008; Jamieson *et al*., 2008; Drahota & Filippi, 2009; Lim *et al*., 2009). Only very few occurrences of such minerals are hosted by rocks other than the gold mine wastes, for example yukonite from the Sterling Hill mine (Dunn, 1982), from Saalfeld, Thüringen, Germany (Ross & Post, 1997), from dolomitic marble deposits at Redziny, Poland (Pieczka *et al*., 1998), from the Venus mine in Yukon, Canada, from the Grotta Della Monaca cave in Italy (Garavelli *et al*., 2009) and the Nalychevskie hot springs, Kamachatka, Russia (Nishikawa *et al*., 2006), Cr-bearing yukonite among the gossans above As-Co-Ni-Ag-Au quartz veins at the Bou Azzer mine, Morocco (Brugger *et al*., 2007), Ca, Fe and Bi arsenates in auriferous oxidized ore at the Ketza River, Yukon, Canada (Thibault & Paktunc, 2008).

The main goal of the present study is the characterization of a Ca–Fe arsenate phase (abbreviated here as CFA) that is intimately associated with an arsenic ferric oxyhydroxide (abbreviated here as AFO). The studied samples were taken from the borehole BTWC-006 at the B'ir Tawilah gold prospect in Saudi Arabia which is currently under extensive subsurface exploration by the Saudi Ma'aden Mining Company. The present work is the first contribution to the occurrence of CFA in the Late Proterozoic Arabo-Nubian Shield as a whole. Also, the present study aims to distinguish between As-ferric oxyhydroxides resulting from oxidation of pyrite and Ca–Fe arsenate pseudomorphing arsenopyrite. The work discusses also the mode of formation of this semicrystalline to amorphous CFA-AFO polyphase aggregate. Such a new finding may furnish better understanding for the so-called ''unidentified Ca–Fe arsenate phases'' in weathered mine tailings (Frau & Ardau, 2004; Jamieson *et al*., 2008; Walker *et al*., 2009a and b), or in weathered samples from drill cores and auriferous bedrocks (Thibault & Paktunc, 2008).

2. Geological set-up of Bi'r Tawilah area

In the late Proterozoic Arabian Shield of Saudi Arabia, the Bi'r Tawilah gold prospect (latitudes 22° 24′ 54″–22° 37′ 11″, longitudes 42° 41′ 14″–42° 45′ 42″) is located along the so-called ''Nabitah suture zone and orogenic belt'' (Fig. 1). According to Schmidt *et al*. (1979) and Stoeser & Camp (1984), the belt represents a 100–200 km wide zone that is dominated by a thick pile of volcanosedimentary sequences of the As Siham group (equivalent to the Hulyfah group in other parts in the Arabian Shield), whereas the younger metasedimentary rocks of the Bani Ghayy group and the ophiolitic mafic-ultramafic rocks define a genuine suture zone between the Afif terrane and the western arc terranes (Stoeser & Camp, 1984). The volcano-sedimentary sequences consist of low-grade schists, metapyroclastics and marble bands. The marble bands occur as sporadic surface exposure and are composed of calcite and very minor diopside and periclase.

The volcanosedimentary rocks of As Siham and Bani Ghayy groups were intruded by syn- to late-orogenic and post-orogenic intrusive rocks. The syn- to late-orogenic intrusive rocks, which mostly occur to the east of Bi'r

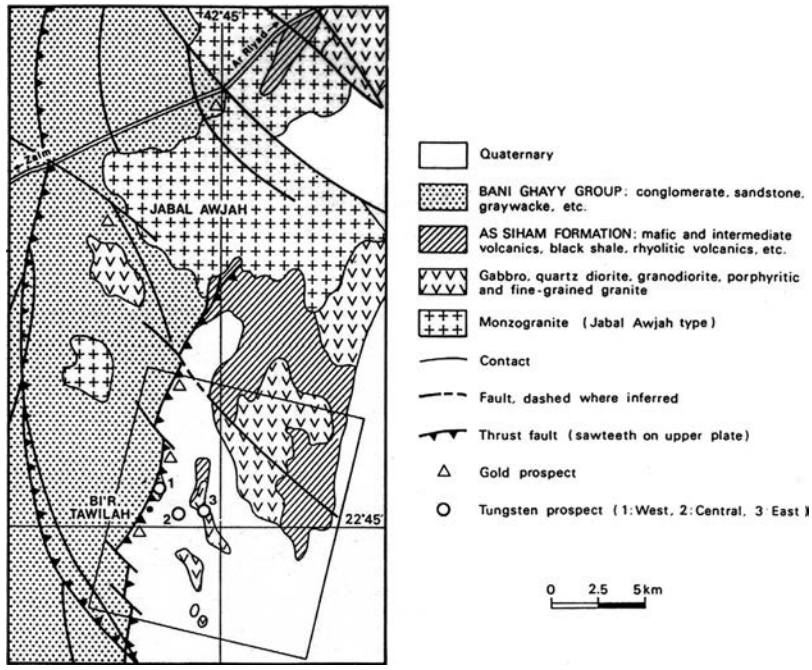

Fig. 1. Geological map of Bi'r Tawilah area (Saber & Labbe, 1986). The exact location of the borehole BTWC-006 that contains arsenate and oxyhydroxide is shown.

Tawilah fault and locally in the central part, range in composition from diorite to granodiorite. The syn-orogenic intrusive rocks are represented by highly weathered, fractured and locally sheared diorite exposed locally to the east of Bi'r Tawilah, while the late varieties are represented by the granodiorite of Jabal Ghadarah which intruded the contact between listwaenitized serpentinite and the late Hulyfah Group rock varieties. The granodiorite is gold-bearing and contains disseminated pyrite and arsenopyrite (Al-Jahdli, 2004).

There are distinct variations in granularity and weathering effect in the granodiorite at different depths. The weathered granodiorite continues until ~19–20 m depth, followed by slightly deformed, less weathered granodiorite (medium- and coarse-grained). Samples of granodiorite below the weathering zones (from ~20 to 205 m) are almost fresh and contain abundant sulphides (mainly pyrite and arsenopyrite) especially in the sheared and brecciated varieties.

3. Methodology

The granodiorite samples used for the present mineralogical studies were collected at the depth interval of ~15–25 m from the ground surface (borehole BTWC-006) in the framework of the Bi'r Tawilah gold prospecting programme by the Saudi Ma'aden Mining Company. The samples were obviously altered and display distinct weathering features if compared to the fresh granodiorite samples at deeper levels. The ore assemblages, as well as the gangue minerals and mutual relationships, were studied using both transmitted and reflected light microscopies. The representative samples were surveyed using the SEM-EDX technique for more detailed identification of minerals and microtextures. The scanning electron microscope with energy dispersive X-ray attachment (SEM-EDX) was a Philips instrument Model XL 30 working at 30 kV accelerating voltage housed at the Central Laboratories of the Egyptian Mineral Resources Authority of Egypt. The quantitative electron microprobe analyses (EPMA) were conducted using a Jeol JXA8200 instrument housed at the Faculty of Earth Sciences, King Abdulaziz University, Jeddah, Saudi Arabia. Operating conditions were 15 kV accelerating voltage, 20 nA probe current and 3 μm beam diameter. The following standards were used: quartz for Si, corundum for Al, periclase for Mg, wollastonite for Ca, pyrite for Fe and S, zircon for Zr, lanthanum phosphate (LaP_5O_{14}) for P, and gallium arsenide (GaAs) for As.

4. Ore paragenesis and paragenetic sequence

Below the oxidation zone in the granodiorite at the Bi'r Tawilah gold prospect, the unweathered samples are rich in primary sulphides (pyrite and arsenopyrite), reaching up to 15 % rock volume. At some boreholes at the prospect, samples of granodiorites brought to the surface from the weathered zone reveal a complex ore paragenesis. The majority is represented by supergene phases in the form of arsenates and oxyhydroxides, in addition to very rare traces of altered magmatic-hydrothermal sulphides and Fe-Ti oxides. The newly studied CFA-AFO polyphase is commonly very fine and stacked to FO. Two brown spots of this polyphase were separated for powder X-ray diffraction (XRD) study. The resultant patterns prove that it is an amorphous to very poorly crystalline phase where almost no peaks can be observed, with the exception of few peaks similar to those of lepidocrocite.

The detailed SEM-EDX investigation allowed to define the micro-textures of the secondary ore minerals well because the microscopic study using the ore microscope was not detailed and just showed the presence of secondary minerals pseudomorphing both pyrite and arsenopyrite. The BSE images show that the altered pyrite (FO) is corroded and partly enclosed by altered arsenopyrite (CFA-AFO) as shown in Fig. 2a, b. The precursor arsenopyrite had either rectangular or rhombic cross-sections. Commonly, the FO hosts native gold as inclusions (~2–10 μm wide) blebs and leaf-like crystals that are confined to either microfractures or the growth planes of its colloform structure. High magnification of the CFA-AFO revealed typical gel-structure (or cellular-like structure) with two distinct domains (Fig. 2c), one is a light domain and the other is dark. Actually, the dark domain itself is distinguished into intermediate and dark domains. The FO replaces pyrite and also partially encloses zircon (Fig. 2d). The remaining accessory minerals are euhedral to subhedral thorite and fine monazite nests (~200 μm wide) where both minerals are enclosed in albite, *i.e*. not in the sulphides. In the unweathered samples of granodiorite, the ore mineral paragenesis is represented by magnetite, rutile, subhedral and euhedral pyrite, euhedral arsenopyrite (Fig. 2e, f) and uncommon anhedral chalcopyrite. Prior to weathering, their paragenetic sequence can be defined as follows: chalcopyrite → pyrite → arsenopyrite, where the amount of arsenopyrite increases with depth.

5. Mineral chemistry

5.1. Ca–Fe arsenate (CFA) and As-rich ferric oxyhydroxide (AFO) polyphase

The electron microprobe analyses (EMPA) of the Ca–Fe arsenate and As-oxyhydroxide polyphase are given in Table 1 that distinguishes the spots in each domain as seen in the BSE images, namely light, intermediate and dark domains. The given EMPA data show clearly that the light domain contains lower SiO_2 content relative to the intermediate and dark domains where silica amounts up to 4.4 wt% and up to 6.8 wt% in the light domain and the dark domain, respectively. The P_2O_5 content in the light domain is almost half of that in the intermediate domain (up to 1.26 wt% and ~2.00–2.43 wt%, respectively). In the light

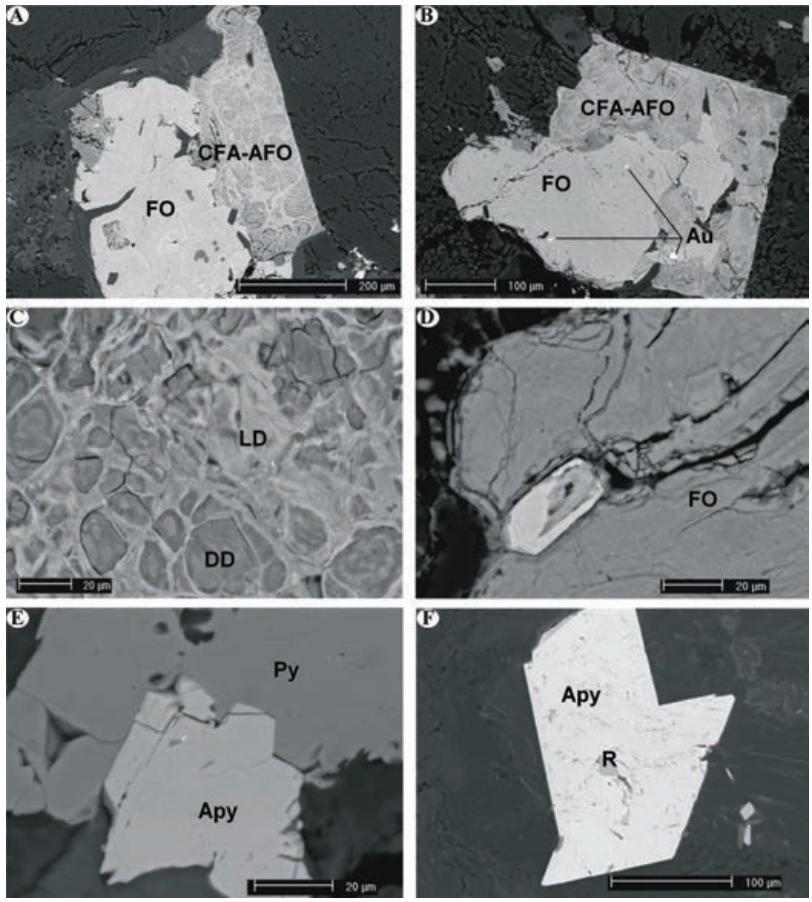

Fig. 2. BSE images of the ore paragenesis in Bi'r Tawilah granodiorite: (a) Composite phase assemblage of mixed CFA-AFO gel-structured phase replacing prismatic arsenopyrite adjacent to FO after pyrite, weathered granodiorite. (b) Composite CFA-AFO showing rhombic outline of pre-existing arsenopyrite partly enclosing FO with native gold specks (Au), weathered granodiorite. (c) Details of the gel-structured CFA-AFO in (a) showing distinct light and dark domains (LD and DD), weathered granodiorite. (d) Zircon inclusion at the outer periphery of colloform FO, weathered granodiorite. (e) Fresh pyrite (Py) and arsenopyrite (Apy), fresh granodiorite. (f) Euhedral rhombic cross-sections of arsenopyrite (Apy) enclosing rutile (R), fresh granodiorite.

domain, there is perfect positive correlation of As_2O_5 with CaO (Fig. 3). This figure shows negative correlations of As_2O_5 with Fe_2O_3 and Fe_2O_3 with CaO as a result of ionic substitutions. Figure 4 suggests also that there are three chemical categories of the light domain that are characterized by definite As_2O_5, CaO and Fe_2O_3 contents that are ~22, 16 and 11 wt%, ~24, 35 and 45 wt% and ~14.5, 10 and 5.5 wt%, respectively.

In the intermediate and dark domains, there is no defined correlation of As_2O_5 with CaO (Fig. 3a) in contrast to the light domain which might attributed to cation disordering and lowering in the pH conditions in the former. As expected, the dark domain is characterized by high Fe_2O_3 content that reaches up to 54.1 wt% (analysis no. 39, Table 1). Actually, the shade of the grey colour in BSE image of the intermediate and dark domains is a function of Fe_2O_3 content where the oxide becomes as low as 48.0 wt% in the former. The given EMPA suggest negligible Mg^{2+} (only a single spot analysis in a dark domain with 0.02 wt% MgO is obtained, analysis no. 29, Table 1). Distribution of Al_2O_3 in all domains is uneven and most probably it is controlled by the dissolution of fine feldspar and mica inclusions. Analyses of spots adjacent to such inclusions contain up to 1.0 wt% alumina.

It was not attempted to calculate structural formulae of the CFA-AFO polyphase because of its amorphous nature and inhomogeneity. For simplicity, the cation number has been determined where it can be roughly normalized on the basis of 25 oxygen atoms in accordance with the chemistry of similar arsenate minerals in literature (*e.g.*, Drahota & Filippi, 2009; Walker *et al*., 2009a; Gomez *et al*., 2010).

5.2. Ferric oxyhydroxide (FO)

Table 2 includes three representative electron microprobe analyses of ferric oxyhydroxide (FO) that pseudomorphs pyrite upon oxidation. One of the prominent chemical signature in the composition is the high Fe_2O_3 content (60.8–63.1 wt%) and the $\{O(OH)\}^2$ anion is considerably high because the structural water presumably amounts ~31–33 wt%. Uncertainty comes from the recent finding

Table 1. Electron microprobe analyses (EMPA) of light, intermediate and dark domains in the studied mixed phase of CFA-AFO.

CFA Light Domain (LD)							AFO Intermediate Domain (ID)								AFO Dark Domain (DD)																		
S.No.	4	7	22	24	36	40	2	3	23	32	33	34	35	41	1	5	6	8	9	10	11	19	20	21	25	26	27	28	29	30	31	38	39
SiO_2	3.48	3.56	3.3	4.38	3.55	4.03	3.22	4.97	2.94	4.38	6.14	5.18	5.08	4.36	4.36	5.3	6.01	4.15	5.71	5.1	5.66	6.5	6.16	6.11	6.57	6.78	5.02	6.46	6.28	5.9	5.82	6.5	4.17
Fe_2O_3	23.94	24.3	34.52	34.73	45.21	45.76	49.46	48.11	52.8	51.21	52.32	48.02	51.98	51.88	50.3	50.79	51.03	52.7	52.01	53.34	51.08	48.47	52.18	50.67	53.01	51.32	53.09	50.66	51.77	52.89	50.55	47.94	54.05
CaO	14.65	14.22	10.56	9.95	5.68	5.43	3.41	4.04	1.96	2.45	3.1	3.6	2.02	2.5	2.38	2.44	2.49	2.54	2.44	2.31	3.03	4.56	3.23	3.96	2.86	2.44	2.53	1.84	3.23	2.12	2.51	2.94	2.06
MgO	n.d.	n.d.	n.d.	n.d.	n.d.	n.d.	n.d.	n.d.	n.d.	n.d.	n.d.	n.d.	n.d.	n.d.	n.d.	n.d.	n.d.	n.d.	n.d.	n.d.	n.d.	n.d.	n.d.	n.d.	n.d.	n.d.	n.d.	n.d.	n.d.	n.d.	n.d.	n.d.	n.d.
Al_2O_3	0.27	0.24	0.3	0.3	0.53	0.32	0.5	0.89	0.4	0.67	0.53	0.42	0.61	0.31	1.01	0.66	0.7	0.59	0.61	0.55	0.78	0.67	0.5	0.63	0.61	0.67	0.42	0.75	0.61	0.67	0.68	0.67	0.32
As_2O_5	22.15	22.25	16.13	15.83	10.67	11.41	8.77	5.4	8.44	8.42	6.18	6.41	7.76	7.62	5.56	6.52	6.01	7.74	5.61	6.52	6.09	5.78	5.94	5.61	5.63	6.06	6.12	5.99	5.82	6.4	6.37	6.26	6.11
P_2O_5	0.23	0.07	0.32	0.34	1.26	0.35	0.24	2.43	0.26	0.38	1.24	1.95	0.2	0.57	0.21	0.12	0.19	0.13	0.08	0.1	1.22	2.02	0.73	1.21	0.6	0.77	1.65	0.77	1.8	0.07	0.74	0.78	0.4
ZrO_2	0.24	0.17	0.16	0.17	0.2	0.09	0.24	0.28	0.02	0.18	0.18	0.16	0.23	0.14	0.29	0.32	0.23	0.26	0.23	0.3	0.22	0.13	0.17	0.16	0.19	0.17	0.05	0.24	0.19	0.3	0.34	0.33	0.04
SO_3	0.05	0.06	0.1	0.1	0.07	0.02	0.08	0.23	0.06	0	0.01	0.05	0.03	0.01	0.11	0.1	0.16	0.12	0.14	0.07	0.17	0.21	0.16	0.17	0.05	0.02	0.02	0.06	0.05	0.02	–	0.01	0.06
Total	65	64.87	65.39	65.79	67.17	67.39	65.92	66.35	66.88	67.68	69.73	65.8	67.91	67.4	64.2	66.24	66.82	68.22	66.83	68.28	68.25	68.35	69.06	68.52	69.52	68.23	68.91	66.75	69.77	68.37	67	65.44	67.2
No. oxygen atoms = 25																																	
Si	1.09	1.12	1.04	1.35	1.08	1.23	1.02	1.49	0.92	1.33	1.78	1.58	1.53	1.33	1.4	1.64	1.82	1.26	1.75	1.53	1.67	1.89	1.8	1.79	1.91	1.99	1.48	1.94	1.8	1.76	1.76	1.99	1.29
Fe	5.64	5.73	8.16	8.07	10.36	10.51	11.75	10.89	12.41	11.7	11.38	11.02	11.79	11.93	12.12	11.8	11.65	12.02	11.95	12.09	11.34	10.58	11.49	11.19	11.59	11.35	11.75	11.46	11.16	11.87	11.48	11.05	12.54
Ca	4.91	4.78	3.56	3.29	1.85	1.78	1.15	1.3	0.66	0.8	0.96	1.18	0.65	0.82	0.82	0.81	0.81	0.82	0.8	0.75	0.96	1.42	1.01	1.24	0.89	0.77	0.8	0.59	0.99	0.68	1	0.96	0.68
Mg	0	0	0	0	0	0	0	0	0	0	0	0	0	0	–	–	–	–	–	–	–	–	–	–	–	–	–	–	0.01	–	–	–	–
Al	0.1	0.09	0.11	0.11	0.19	0.12	0.19	0.32	0.15	0.24	0.18	0.15	0.22	0.11	0.38	0.24	0.25	0.21	0.22	0.2	0.27	0.23	0.17	0.22	0.21	0.23	0.15	0.26	0.21	0.24	0.24	0.24	0.11
As	3.62	3.65	2.65	2.56	1.7	1.82	1.45	0.85	1.38	1.34	0.93	1.02	1.22	1.22	0.93	1.05	0.09	1.23	0.9	1.03	0.94	0.88	0.91	0.86	0.86	0.93	0.94	0.94	0.87	1	1.01	1	0.98
P	0.06	0.02	0.08	0.09	0.33	0.09	0.06	0.62	0.07	0.1	0.3	0.5	0.05	0.15	0.06	0.03	5.00	0.03	0.02	0.02	0.3	0.5	0.18	0.3	0.15	0.19	0.41	0.2	0.44	0.02	0.19	0.2	0.1
Zr	0.04	0.03	0.02	0.03	0.03	0.01	0.04	0.04	0	0.03	0.02	0.02	0.03	0.02	0.04	0.05	0.03	0.04	0.03	0.04	10.0	0.02	0.02	0.02	0.03	0.02	0.01	0.03	0.03	0.04	0.05	0.05	0.01
S	0.01	0.01	0.02	0.02	0.02	0	0.02	0.05	0.01	0	0	0.01	0.01	0	0.03	0.02	0.04	0.03	0.03	0.02	0.04	0.04	0.04	0.04	0.01	0	0.01	0.01	0.01	0	–	0	0.01
Total	15.46	15.42	15.65	15.52	15.55	15.57	15.67	15.56	15.6	15.53	15.56	15.5	15.51	15.58	15.77	15.63	15.61	15.64	15.7	15.67	15.55	15.54	15.63	15.66	15.64	15.5	15.53	15.44	15.51	15.61	15.54	15.5	15.72

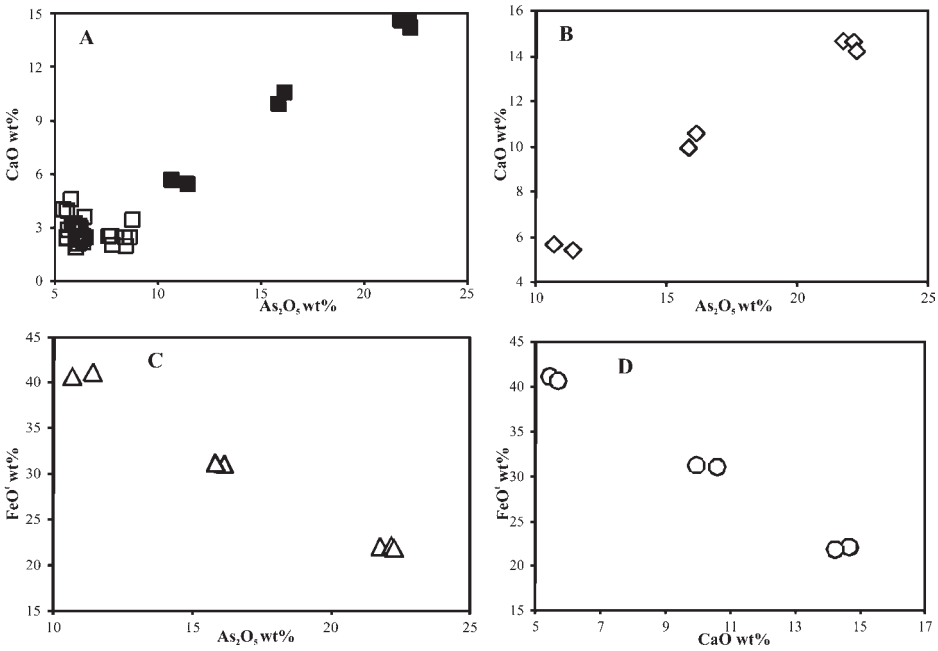

Fig. 3. (a) Perfect positive correlation of As_2O_5 *vs*. CaO in the light domains of Bi'r Tawilah CFA (closed squares). Notice ill-defined correlations for intermediate and dark domains (open squares). (b–d) show the positive (As_2O_5 *vs*. CaO) and negative correlations (FeOt *vs*. As_2O_5 and CaO *vs*. FeOt) in the light domain only.

Table 2. EMPA of accessory mineral inclusions in ferric oxyhydroxide (FO) and EDS analyses of monazite and thorite inclusions in feldspars.[a]

	Oxyhydroxides			Apatite		Albite	Chlorite	Monazite	Thorite	
S.No.	13	14	15	16	17	18	37	54	56	57
SiO_2	3.12	2.48	2.81	0.18	0.12	66.18	43.42		17.78	17.05
FeO	60.81	63.13	62.41	1.53	1.27	1.17	7.6			
CaO	0.8	0.65	0.7	55.15	55.5	0.03	0.13			
MgO	0.32	0.43	0.37		0.03		12.19			
Al_2O_3	0.38	0.34	0.42	0.02	0.01	18.13	20.74			
As_2O_5	1.28	1.21	1.47		0.01	0	0.12		15.39	10.99
P_2O_5	0.02	0.08	0.12	42.69	44.32		0.16	33.16		
ZrO_2	0.02	0.01	0.01	0.06	0.03		0.05			
SO_3	0.05	0.03	0.06	0.11	0.08		0			
ThO_2									66.84	71.95
La_2O_3								18.9		
Ce_2O_3								34.65		
Nd_2O_3								13.29		
Total	66.78	68.35	68.37	99.73	101.34	85.51	84.42	100	100	100

[a]Blanks mean that the elements were not detected.

of Xu *et al*. (2011) that suggests that ferrihydroxide or ferric oxyhydroxide contains very little structural water where the molar ratio of OH/Fe is 0.18 ± 0.01. The presumably given ferric oxide and water contents of the Bi'r Tawilah FO are much higher than in common HFO (hydrated ferric oxides) associating Ca–Fe arsenates in gold mine tailings elsewhere in the world (e.g., Walker *et al*., 2009a).

The analyses of FO formed at the expense of pyrite (Table 2) have the lowest silica content if compared to the mixed CFA-AFO phase that replaces arsenopyrite. SiO_2 in FO amounts 2.81–3.17 wt%. Also, CaO is the least (0.65–0.80 wt%) but with some considerable traces of MgO (0.32–0.43 wt%) indicating ionic substitution of Mg^{2+} for Ca^{2+}. In the FO, there is appreciable amount of As_2O_5 (1.21–1.47 wt%) whereas there is very little traces of S (SO_3^{2-} <0.06 wt%) suggesting very pervasive replacement of the precursor pyrite. On experimental basis, García-Sanchez *et al*. (2002) documented common adsorption of As^{5+} by ferric oxyhydroxides.

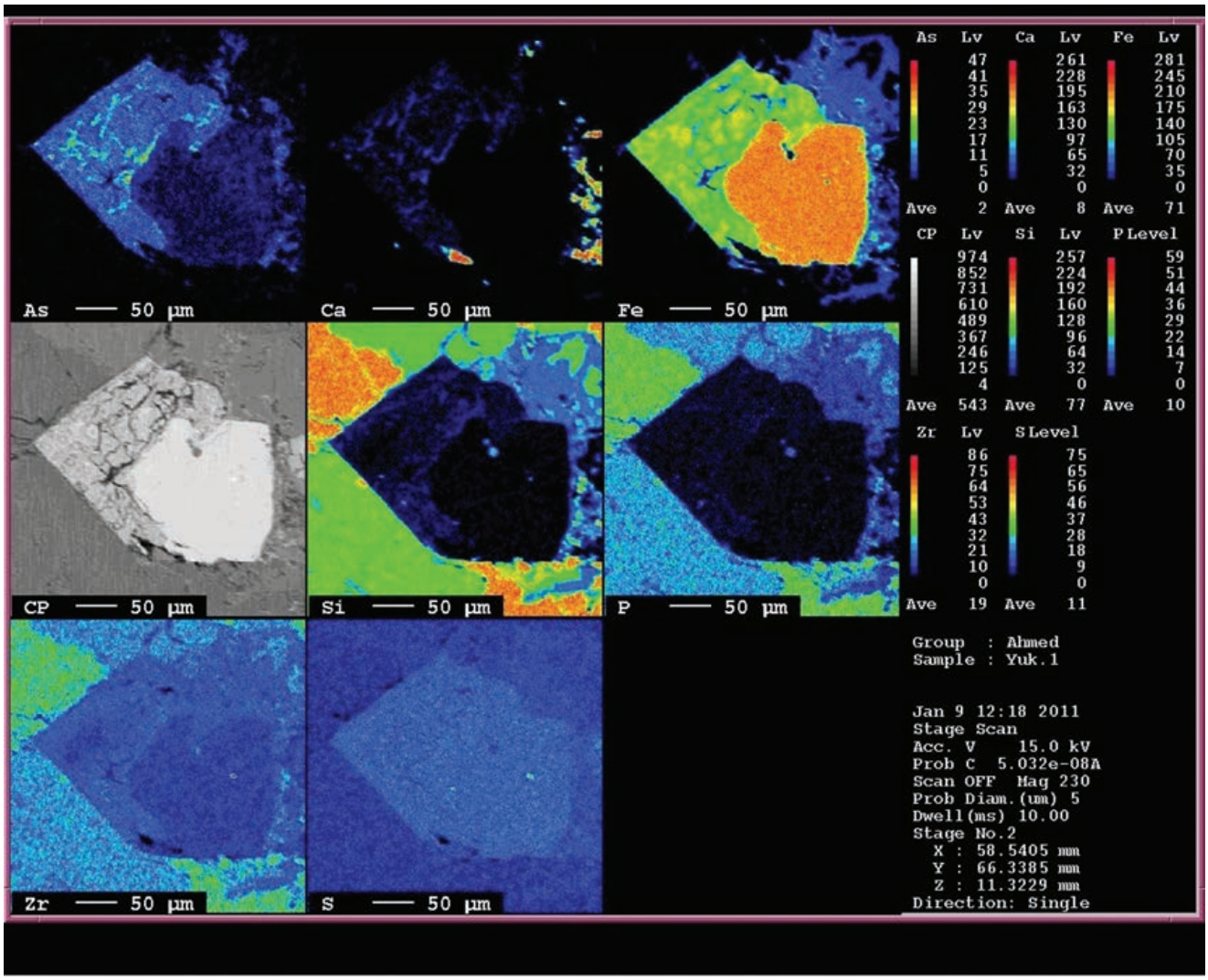

Fig. 4. Element distribution map of a composite mixed CFA-AFO phase after arsenopyrite (left) and FO after pyrite (right). CP is the BSE image of the analyzed crystals.

The element distribution map of the CFA-AFO phase adjacent to FO (Fig. 4) shows distinct chemical variations between the two parts of such inhomogeneous polyphase aggregate. Distribution of As, Ca and Fe in the CFA-AFO mixed phase is inhomogeneous. The figure indicates also an uneven distribution of Si, P and Zr in the CFA-FO part whereas these elements are relatively enriched in the FO. Generally, S is almost absent in all phases indicating pervasive oxidation of composite pyrite-arsenopyrite crystals during weathering of the granodiorite host and removal of nearly all sulphates.

6. Discussion

The weathered granodiorite that includes the studied arsenate and oxyhydroxides are only confined to the upper horizon of a huge granodiorite body where the investigated samples were collected at about 16 m below water level from a borehole. The continuation of weathering downwards can be traced only up to a depth of ~20 m and the deeper granodiorite samples are almost fresh. Similar to the studied granodiorite, Al-Jahdli (2004) reported a nearby granodiorite body adjacent to listwaenite at Jabal Ghadarah where the weathered granodiorite is auriferous and contains native gold. Hence, it is believed that at both Bi'r Tawilah and Jabal Ghadarah the granodiorite was chemically weathered and led to the liberation of invisible gold from the contained sulphides upon oxidation. It can be attributed to low temperature weathering and its timing is recent after uplift of the whole basement mass. Textures, mineral paragenesis and chemistry of the studied Ca–Fe arsenate (CFA) and arsenian ferric oxyhydroxide (AFO) suggests that weathering was active at prevailing high pH conditions ($\geq$8) based on the mineral stability fields given by Sigel *et al.* (2005). The resultant ''gel-like'' CFA and AFO polyphase is characterized by cellular structure. The gel-like structure can be explained in terms

of oxidation reaction kinetics of the arsenopyrite and the co-existing pyrite. Major controls are pH and the rate of ion diffusion (Ca^{2+}, Fe^{3+} and As^{5+}) contemporaneous to the development of the mixed or intergrown CFA-AFO phase. Appearance and inhomogeneity of this mixed phase suggest that it is amorphous or very poorly crystalline, and originated from the colloidal state similar to several Ca–Fe arsenate occurrences elsewhere in the world, e.g. USA, Canada, Russia, Poland and Spain (Ross & Post, 1997; Pieczka *et al*., 1998; Golębiowska *et al*., 2001; Murciego *et al*., 2009).

During the last two decades, some experimental works contributed to the Ca–Fe(III)–As(V) system, involving synthesis, characterization and preliminary solubility testing of Ca–Fe(III)–As(V) compounds, *e.g.* Robins *et al*. (1988), Waychunas *et al*. (1993), Swash & Monhemius (1995), Moldovan *et al*. (2003), and Jia & Demopoulos (2008). Direct precipitation from a gypsum-saturated matrix solution in the presence of calcite at pH 8 and 75–95 °C leads to the formation of crystalline yukonite and kolfanite (Becze & Demopoulos, 2007; Jia & Demopoulos, 2008).

At the Bi'r Tawilah prospect, the intimate association of CFA, AFO and FO phases suggests that As retention in the CFA is manifested by the co-precipitation of oxyhydroxides. The increase of oxyhydroxide (or ferrihydrite) precipitation at pH = 7 is responsible for maximum destabilization of scorodite (Paktunc & Bruggeman, 2010). The main view regarding arsenate speciation in coprecipitates is that arsenate is adsorbed via surface complex formation on ferrihydrite or oxyhydroxides (Harris & Monette, 1988; Robins *et al*., 1988; Waychunas *et al*., 1993; Moldovan *et al*., 2003; Richmond *et al*., 2004; Moldovan & Hendry, 2005). Also, this is supported by the coprecipitation studies involving either low arsenic concentrations or elevated pH 8–9.8 (Waychunas *et al*., 1993; Moldovan *et al*., 2003). Scorodite is missed among the mineral assemblage at Bi'r Tawilah, which is a strong evidence of high pH and temperature during weathering that led to the formation of CFA instead of scorodite. Experimentally, Demopoulos (2005) proved that Ca–Fe arsenates form by the dissolution of scorodite at 75 °C, pH 7 in the presence of gypsum. Owing to the lack of sulphates in the mineral assemblage at Bi'r Tawilah, and based on the experimental work of Jia & Demopoulos (2008), the pH $\geq$ 8.

Oxidation of arsenopyrite at elevated pH results in the following: i) the transformation of As^{3+} to As^{5+}, and ii) its fixation in the newly formed CFA phase. Oxidation of arsenopyrite at pH as low as $\leq$3 leads to As^{3+} mobilization and its accumulation in the pore fluids and ground waters (Pereira de Andrade *et al*., 2008). At Bi'r Tawilah, destabilization of arsenopyrite is late and associates the main oxidizing events during weathering and this is greatly enhanced by the earlier oxidation of co-existing pyrite. There is consensus among workers that iron in either amorphous or crystalline CFA phases is ferric, and this is supported also by some Mössbauer spectra that reveal typical Fe^{3+} coordinating oxygen atoms and OH^- whereas Fe^{2+} is completely absent in the structure (Golębiowska *et al*., 2001).

Yu *et al*. (2007) proved experimentally that the release rate of As^{5+} in this previous reaction is favourable at a pH value in the range of 7–8 which may have been due to oxidation of Fe^{2+} to Fe^{3+} and availability of H^+ to form hydrous ferric oxides (HFO). Concerning the weathering products of pyrite and formation of ferric oxyhydroxides, there is a series of reactions during oxidation of Fe-bearing sulphide minerals that leads to the transformation of Fe^{2+} to Fe^{3+} and furnishes sulphate ions. Such series of reactions were summarized by Boorman & Watson (1976) and Blowes (1997). In summary, destabilization of sulphides starts with the transformation of pyrite to amorphous oxyhydroxides, and then arsenopyrite is transformed into scorodite in acidic condition during the major oxidizing event, and finally scorodite is destabilized to amorphous Ca–Fe arsenate with increasing pH in the alkaline pore fluids. The case study at the Bi'r Tawilah prospect seems to be analogous to similar auriferous oxidized ore samples at the Ketza River mine in Canada (Thibault & Paktunc, 2008). What is new here in the present study is the detailed mineralogical and chemical characterization of the amorphous Ca–Fe arsenate phase. Finally, the pre-existing scorodite was destabilized by the alkaline pore fluids with high pH buffered by the dissolution of calcite from the limestone and marble wallrock at the Ketza River mine and at the Bi'r Tawilah prospect, respectively.

7. Conclusions

The newly recorded amorphous to very poorly crystalline CAF-AFO polyphase was formed by *in situ* weathering of granodiorite where primary pyrite and arsenopyrite were destabilized. The light domains (CFA) is not an arsenosiderite and neither scorodite nor yukonite. Elevated pH (as high as 8) and temperatures up to 75 °C during oxidation of As-Fe sulphides in the granodiorite at the Bi'r Tawilah were responsible for the conversion of a pre-existing hydrated Fe-arsenate phase (scorodite) to a chemically inhomogeneous CFA-AFO phase. It is evident that availability of Ca^{2+} leached from altered plagioclase and marble bands, relatively high pH value and the prevailing high temperature played important roles in the formation of the amorphous to very poorly crystalline brown CFA-AFO polyphase at Bi'r Tawilah. On optical and mineral chemistry bases, the present authors were able to distinguish AFO (arsenic ferric oxyhydroxide intergrown with CFA, Ca–Fe arsenate pseudomorphing arsenopyrite) from FO (ferric oxyhydroxide, pseudomorphing pyrite).

Acknowledgements: The authors are greatly indebted to the Saudi Mining Company (Ma'aden) for hospitality and generous logistic support offered by Tewolde Woldeabzghi. Also, we would like to thank Munir Noor and Sami Al Harbi for providing us and some of our undergraduate students with samples from the borehole BTWC-006 at the Bi'r

Tawilah gold prospect. Other geologists at the prospect site shared some valuable discussions on history of mineralization and ore exploration with the authors. Sandro Conticelli is thanked for his editorial handling. The manuscript benefited from the thorough reviews and improvements by Marcello Mellini and Uwe Kolitsch.

References

Al-Jahdli, N.S. (2004): Geology of Jabal Ghadarah area, Bi'rTawilah district with special emphasis on listvinite as a potential source for gold in the Kingdom of Saudi Arabia. MSc thesis, King Abdulaziz University, Jeddah, Saudi Arabia.

Becze, L. & Demopoulos, G.P. (2007): Hydrometallurgical synthesis and stability evaluation of Ca–Fe–AsO_4 compounds. *In* ''TMS 2007'', B. Davis, M.L. Free, eds. 136th Annual Meeting and Exhibition the Minerals, Metals and Materials Society, Orlando, FL.

Blowes, D.W. (1997): The environmental effects of mine wastes. *in* ''The Proceedings of Exploration 97'', A.G. Gubins, ed. The 4th Decennial International Conference on Mineral Exploration, Prospectors and Developers Association of Canada, 887–892.

Boorman, R.S. & Watson, D.M. (1976): Chemical processes in abandoned sulphide tailings dumps and environmental implications for the Northwestern New Brunswick. *Can. Inst. Min. Bull*., **69**, 86–96.

Brugger, J., Meisser, N., Krivovichev, S., Armbuster, T., Favreau, G. (2007): Mineralogy and crystal structure of bouazzerite from BouAzzer, Anti-Atlas, Morocco: Bi-As-Fe nanoclusters containing Fe^{3+} in trigonal prismatic coordination. *Am. Mineral*., **92**, 1630–1639.

Cano-Aguilera, B.E., Rubio-Campos, B.E., De la Rosa, G., Aguilera-Alvarado, A.F. (2008): Arsenic mobility from mining tailings of Monte San Nicolas to Presa de Mata in Guanajuato, Mexico. *Engineering Technol*., **47**, 390–393.

Demopoulos, G.P. (2005): On the preparation and stability of scorodite. *In* ''Arsenic metallurgy'', R.G. Reddy, V. Ramachandran, eds., TMS, Warrendale, PA, 25–50.

Drahota, P. & Filippi, M. (2009): Secondary arsenic minerals in the environment: a review. *Environ. Int*., **35**, 1243–1255.

Dunn, P.J. (1979): Contributions to the mineralogy of Franklin and Sterling Hill, New Jersey. *Mineral. Record*, **10**, 160–165.

— (1982): New data for pitticite and a second occurrence of yukonite at Sterling Hill, New Jersey. *Mineral. Mag*., **46**, 261–264.

Filippi, M., Doušová, B., Machovič, V. (2007): Mineralogical speciation of arsenic in soil above the Mokrsko-west gold deposit, Czech Republic. *Geoderma*, **139**, 154–170.

Frau, F. & Ardau, C. (2004): Mineralogical controls on arsenic mobility in the Baccu Locci stream catchment (Sardinia, Italy) affected by past mining. *Mineral Mag.*, **68**, 15–30.

Garavelli, A., Pinto, D., Vurro, F., Mellini, M., Viti, C., Balić-Žunic, T., Della Ventura, G. (2009): Yukonite from the Grotta Della Monaca cave, Sant'agata di Esaro, Italy: characterization and comparison with cotype material from the Daulton mine, Yukon, Canada. *Can. Mineral*., **47**, 39–51.

García-Sanchez, A., Alvarez-Ayuso, E., Rodriguiz-Martin, F. (2002): Sorption of As(V) by some oxyhydroxides and clay minerals. Application to its immobilization in two polluted mining soils. *Clay Minerals*, **37**, 187–194.

Golębiowska, B., Pieczka, A., Zabiniski, W. (2001): Spectroscopic study of yukonite (Ca–Fe arsenate mineral). *in* ''The 4th European Conference on Mineral Spectroscopy, Extended Abstracts'', Bull. Liaison, **13**, 78–79.

Gomez, M.A., Becze, L., Demopoulos, G.P., Assaaoudi, H., Cutler J.N., Blyth, R.I.R. (2009): Characterization of Ca–Fe(III)–AsO_4–SO_4 phases relating to arsenic disposal in hydrometallurgical operations. Chemical and Materials Science, Canadian Light Source, 2008 Activity Report, 62–63.

Gomez, M.A., Becze, L., Blyth, R.I.R., Cutler, J.N., Demopoulos, G.P. (2010): Molecular and structural investigation of yukonite (synthetic & natural) and its relation to arsenosiderite. *Geochim. Cosmochim. Acta*, **74**, 5835–5851.

Harris, G.B. & Monette, S. (1988): The stability of arsenic-bearing residues. *In* ''Arsenic metallurgy: fundamentals and applications'', R.G. Reddy, J.L. Hendrix, P.B. Queneau, eds., TMS, Warrendale, PA, 469–498.

Jambor, J.L. (1966): Re-examination of yukonite. *Can. Mineral.*, **8**, 667.

Jamieson, H.E., Walker, M.B., Parsons, M.B., Hall, G.E.M. (2008): Characterization of multiple secondary minerals in arsenic-rich gold mine tailing. *Goldschmidt Conf. Abst*., A 424.

Jia, Y. & Demopoulos, G.P. (2008): Coprecipitation of arsenate with iron(III) in aqueous sulfate media: Effect of time, lime as base and co-ions on arsenic retention. *Water Res*., **42**, 661–668.

Juillot, F., Ildefonse, Ph., Morin, G., Calas, G., Lersabiec, A.M. (1999): Remobilization of arsenic from buried wastes at an industrial site: mineralogical and geochemical control. *Appl. Geochem*., **14**, 1031–1048.

Lim, M., Han, G.-C., Ahn, J.-W., You, K.-S., Kim, H.-S. (2009): Leachability of arsenic and heavy metals from mine tailings of abandoned mines. *Int. J. Environ. Res. Public Health*, **6**, 2865–2879.

Moldovan, B.J. & Hendry, M.J. (2005): Characterizing and quantifying controls on arsenic solubility over a pH range of 1–11 in a uranium mill-scale experiment. *Environ. Sci. Technol*., **39**, 4913–4920.

Moldovan, B.J., Jiang, D.T., Hendry, M.J. (2003) Mineralogical characterization of arsenic in uranium mine tailings precipitated from iron-rich hydrometallurgical solutions. *Environ. Sci. Technol*., **37**, 873–879.

Murciego, A.M., Pascual, E.P., Rodríguez, M.A., Álvarez-Ayuso, E., García-Sánchez, A., Rubio, F., Rubio, J. (2009): Arsenopyrite weathering products in Barruecopardo mine tailings (Salamanca, Spain). *Rev. Soc. Mineral*., **11**, 133–134.

Nishikawa, O., Okrugin, V., Belkova, N., Saji, I., Shiraki, K., Tazaki, K. (2006): Crystal symmetry and chemical composition of yukonite: TEM study of specimens collected from Nalychevskie hot springs, Kamchatka, Russia and from Venus mine, Yukon Territory, Canada. *Mineral. Mag*., **70**, 73–81.

Paktunc, D. & Bruggeman, K (2010): Solubility of nanocrystalline scorodite and amorphous ferric arsenate: Implications for stabilization of arsenic in mine wastes. *Appl. Geochem*., **25**, 674–683.

Pereira de Andrade, R.P., Filho, S.S., Vargas de Mello, J.W., Ribeiro de Figueiredo, B., Dussin, T.M. (2008): Arsenic mobilization from sulfidic materials from gold mines in Minas Gerais State. *Química Nova*, **31**, 1127–1130.

Pieczka, A., Golębiowska, B., Franus, W. (1998): Yukonite, a rare Ca–Fe arsenate from Redziny (Sudetes, Poland). *Eur. J. Mineral.*, **10**, 1367–1370.

Richmond, W.R., Loan, M., Morton, J., Parkinson, G.M. (2004): Arsenic removal from aqueous solution via ferrihydrite crystallization control. *Environ. Sci. Technol*., **38**, 2368–2372.

Roberts, A.C., Cooper, M.A., Hawthorne, F.C., Criddle, A.J., Stirling, J.A.R. (2002): Sewardite, $CaFe^{3+}{}_2(AsO_4)_2(OH)_2$, the Ca-analogue of carminite, from Tsumeb, Namibia: description and crystal structure. *Can. Mineral.*, **40**, 1191–1198.

Robins, R.G., Huang, J.C.Y., Nishimura, T., Khoe, G.H. (1988): The adsorption of arsenate ion by ferric hydroxide. *In* ''Arsenic Metallurgy: Fundamentals and Applications'', R.G. Reddy, J.L. Hendrix, P.B. Queneau, eds., TMS, Warrendale, PA, 99–112.

Ross, D.R. & Post, J.E. (1997): New data on yukonite. *Powder Diffraction*, **12**, 113–116.

Saber, H. & Labbe, J.-F. (1986): Bi'r Tawilah tungsten prospect, Najd region, Kingdom of Saudi Arabia. *J. Afr. Earth Sci*., **4**, 249–255.

Salzsauler, K.A., Sidenko, N.V., Sherriff, B.L. (2005): Arsenic mobility in alteration products of sulfide-rich, arsenopyrite-bearing mine wastes, Snow Lake, Manitoba, Canada. *Appl. Geochem*., **20**, 2303–2314.

Saxena, V.K., Kumar, S., Singh, V.S. (2004): Occurrence, behaviour and speciation of arsenic in groundwater. *Curr. Sci*., **86**, 281–284.

Schmidt, D.L., Hadley, D.G., Stoeser, D.B. (1979): Late Proterozoic crustal history of the Saudi Arabian Shield, Southern Najd Province, Kingdom of Saudi Arabia. *in* ''Evolution and mineralization in the Arabian-Nubian Shield'', A.M.S. Al Shanti, ed., *King Abdulaziz Univ., Inst. Appl. Geol. Bull.*, **3**, 41–58.

Shuvaeva, O.V., Bortnikova, S.B., Korda, T.M., Lazareva, E.V. (2007): Arsenic speciation in contaminated gold processing tailings dam. *Geostand. Geoanal. Res*., **24**, 247–252.

Sigafusson, B., Meharg, A.A., Gislason, S.R. (2008): Regulation of arsenic mobility on basaltic surfaces by speciation and pH. *Environ. Sci. Technol*., **42**, 8816–8821.

Sigel, A., Sigel, H., Sigel, R.K.O. (2005): Metal ions on biological systems. Biogeochemistry, availability and transport of metals in the environment, vol. 44. Taylor and Francis Group, Boca Raton, FL, 307 p.

Stoeser, D.B & Camp, V.E. (1984): Pan-African microplate accretion of the Arabian Shield. Saudi Arabian Deputy Ministry for Mineral Resources. Technical Record, USGS-TR-04-17.

Swash, P.M. & Monhemius, A.J. (1995): Synthesis, characterisation and solubility testing of solids in the $Ca–Fe–AsO_4$ system. Mining and the environment. *in* Proceedings from Sudbury '95, May 28–June 1, Sudbury, ON.

Thibault, Y. & Paktunc, D. (2008): Evolution of arsenic mineralogy through sulfide oxidation at the Ketza River mine, Yukon, Canada. *Goldschmidt Conf. Abst*., A943.

Tyrrell, J.B. & Graham, R.P.D. (1913): Yukonite, a new hydrous arsenate of iron and calcium from Tagish Lake, Yukon territory, Canada: with a note on the associated symplesite. *Trans. R. Soc. Canada, Sec. No. 4*, **7**, 13–18.

Walenta, K. (1998): Ein neues arsenosideritähnliches Mineral aus dem Schwarzwald. *Der Erzgräber*, **12**, 41–48.

Walker, S.R., Parsons, M.B., Jamieson, H.E., Lanzirotti, A. (2009a): Arsenic mineralogy of near-surface tailings and soils: influences on arsenic mobility and bioaccessibility in the Nova Scotia gold mining districts. *Can. Mineral*., **47**, 533–556.

Walker, S.R., Parsons, M.B., Jamieson, H.E. (2009b): Arsenic mineralogy and potential for accessibility in weathered gold mine tailings from Nova Scotia. *in* Proceedings of the 24th International Applied Geochemistry Symposium (IAGS), Fredericton, New Brunswick, Canada, 931–934.

Waychunas, G.A., Rea, C.B.A., Fuller, C., Davis, J.A. (1993): Surface chemistry of ferrihydrite: Part 1. EXAFS studies of the geometry of coprecipitated and adsorbed arsenate. *Geochim. Cosmochim. Acta*, **57**, 2251–2269.

Xu, W., Hausner, D.B., Harrington, R., Lee, P.L., Strongin, D.R., Parise, J.B. (2011): Structural water in ferrihydroxide and constraints this provides on possible structural models. *Am. Mineral*., **96**, 513–520.

Yu, Y., Zhu, Y., Gao, givenname>Z., Gammons, C.H., Li, D. (2007): Rates of arsenopyrite oxidation and Fe(III) at pH 1.8–12.6 and 15–45 °C. *Environ. Sci. Technol*., **41**, 6460–6464.

Received 16 February 2012
Modified version received 23 July 2012
Accepted 25 September 2012